Supporting Information

Cooperative defect engineering and ligand modification in UiO-66 to achieve high proton conductivity

Xiao-Min Li[a†], Junchao Jia[a†], Mingyang Zhao[a], Dongbo Liu[a], Junkuo Gao[*a], Ya-Qian Lan[*b]

a Institute of Functional Porous Materials, School of Materials Science and Engineering, Zhejiang Sci-Tech University, Hangzhou 310018, P. R. China.

E-mail: jkgao@zstu.edu.cn

b School of Chemistry, South China Normal University, Guangzhou, Guangdong 510006, P. R. China.

E-mail: yqlan@m.scnu.edu.cn

† These authors contributed equally to this work.

Table of contents

1. Materials and methods

1.1 Materials preparation

Chemicals: All reagents used in this study were analytical grade and without further purification. All solutions used in this study were prepared with deionized (DI) water (resistivity ≥18.2 MΩ, Millipore Milli-Q). 2-Aminoterephthalic acid (BDC-NH_2) and 1H-imidazole-2-carboxaldehyde were obtained from Bidepharm. $ZrCl_4$ was obtained from Macklin. N, N-dimethylformamide (DMF), acetic acid (CH_3COOH), acetone (CH_3COCH_3), ethanol absolute (CH_3CH_2OH) and methanol absolute (CH_3OH) were purchased from Sinopharm Chemical Reagent Co. Ltd.

Synthesis of UiO-66-NH_2[1]: $ZrCl_4$ (0.240 g) and BDC-NH_2 (0.186 g) were dissolved in 60 mL DMF and heated in an oven at 120 ℃ for 48 h. After cooling to room temperature, the solid was collected and washed with DMF (30 mL × 3) and methanol absolute (30 mL × 3). Then the obtained solid was immersed in methanol overnight. The next day, the product was centrifuged and dried in a vacuum oven at 80 ℃.

Synthesis of D-UiO-66-NH_2[2]: $ZrCl_4$ (0.192 g) and BDC-NH_2 (0.148 g) were dissolved in 24 mL DMF, respectively. Then the two obtained solutions were mixed with 40 μL H_2O and 9.44 mL acetic acid and then was heated in an oven at 120 ℃ for 24 h. After cooling to room temperature, the solid was collected and washed with DMF (30 mL × 6) and then exchanged with acetone for 2 days (change the solvent three times a day). Finally, the product was centrifuged and dried in an oven at 180 °C for 12h.

Synthesis of UiO-66-N=IM[3]: 1H-imidazole-2-carboxaldehyde (0.0673 g) was dissolved in 30 mL ethanol absolute, then 0.235 g UiO-66-NH_2 was added into the above liquid. The mixed liquid was subsequently loaded into a 100 mL three-neck flask and refluxed at 80 ℃ for 24 h. Finally, the product was centrifuged and washed with ethanol absolute (30mL × 3) and then dried in a vacuum oven at 80 °C.

Synthesis of D-UiO-66-N=IM: Similarly, D-UiO-66-NH_2 was dried in an oven at 120 ℃ for 12 h. 1H-imidazole-2-carboxaldehyde (0.1 g) was dissolved in 30 mL ethanol absolute, then 0.2 g D-UiO-66-NH_2 was added into the above liquid. The mixed liquid was subsequently loaded into a 100 mL three-neck flask and refluxed at 80 ℃ for 24 h. Finally, the product was centrifuged and washed with ethanol absolute (30 mL × 3) and

then dried in a vacuum oven at 80 °C.

1.2 Characterization methods

Powder X-ray diffraction data (PXRD) were recorded on a Bruker D8 Advance diffractometer using a graphite-monochromatized Cu Kα (λ = 1.5418 Å) radiation, and the measured parameter included a scan speed of 5° min^{-1} and a scan range of 2θ from 5 to 50°. Thermogravimetric analysis (TGA) was conducted on a NETZSCH TG 209 F1 apparatus with a heating rate of 10 °C min^{-1} from ambient temperature to 900 °C. N_2 adsorption-desorption isotherms were measured at 77 K on an ASAP 2020 HD88. The samples were activated under N_2 stream at 120 °C for 12 h. Morphology analysis of the composite materials was examined by a scanning electron microscope (GeminiSEM 500). Energy-dispersive X-ray spectroscopy (EDS) and elemental mapping were also performed with GeminiSEM 500. The Fourier transform infrared (FTIR) data were collected by a Fourier transform infrared spectrometer (Nicolet 5700, Thermo Electron Corp., USA) in the range of 4000−400 cm^{-1}. H_2O adsorption-desorption isotherms were measured at 298K on a Quantachrome Instruments Autosorb AS-6B. The ^1H NMR spectra were performed by a Bruker 400 MHz spectrometer with NaOD as digestion solvent.

1.3 Acid-base titration method

For D-UiO-66-NH_2, there are three types of protons involved in the reaction: μ_3-OH，-OH_2，-OH. The acid-base titration curve shows three inflection points, which may correspond to the three types of protons. The first-derivative curve is used to determine the equivalence points in the titration curve. The first point can be assigned to the μ_3-OH proton. The other protons correspond to defect sites in the node. The second point and the third point correspond to the Zr-OH_2 proton and Zr-OH proton, respectively.

2. Proton conductivity measurements

Firstly, the powder samples were put into a self-made mold with a radius of 0.2 cm for compression to obtain circular pellets and their thicknesses were determined by a vernier caliper. Secondly, the tablet was clipped with two pieces of gold and then the test clamp was placed on a double glass beaker container for test. Different saturated salt solutions ($MgCl_2$, 33% RH; K_2CO_3, 43% RH; $Mg(NO_2)_3$, 53% RH; $NaNO_2$, 63%

RH; NaCl, 75% RH; KCl, 85% RH; Na_2SO_4, 93% RH) or pure water (100% RH) was used to control the relative humidity. Circulating water with controlled temperature was used to tune the temperature. The alternating current (AC) impedance data were recorded using an electrochemical workstation with a voltage of 100 mV, and the frequency range was 1 MHz ~1 Hz at 30-70 °C. The proton conductivity (σ/S cm^{-1}) was calculated using the following equation.

$$\sigma = \frac{l}{SR}$$

where *σ, l, S* and *R* mean the conductivity (S cm^{-1}), the thickness (cm) of the pellet, the cross-sectional area (cm^2) of the pellet and the bulk resistance (*Ω*), respectively. The activation energy (*E*a) was calculated from the following equation

$$ln\sigma_T = ln\sigma_0 - \frac{E_a}{KT}$$

where *σ, K* and *T* mean the conductivity (S cm^{-1}), the Boltzmann constant (eV / K) and the temperature (*K*), respectively. ZView software was used to get bulk resistance by fitting the semicircle of Nyquist plots and the values of conductivity and activated energy were obtained by calculation following the above equations.

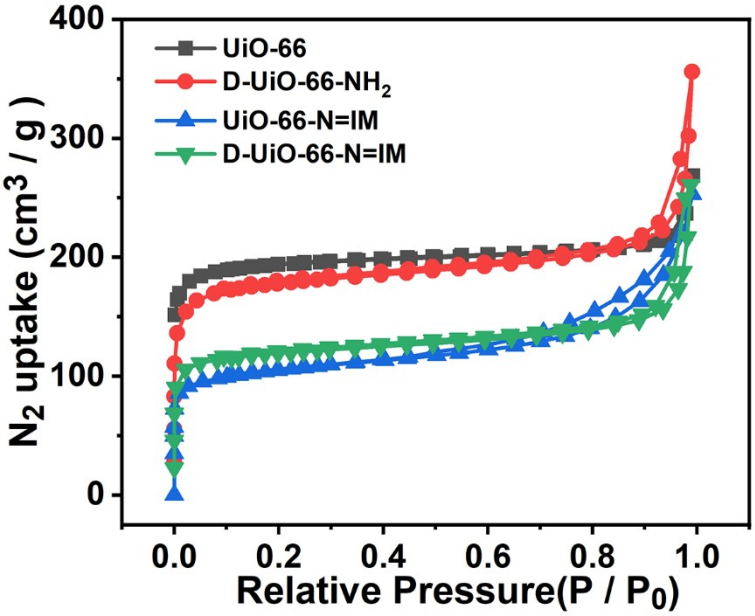

Fig. S1. N_2 adsorption-desorption isotherms of UiO-66 (gray), D-UiO-66-NH_2 (red), UiO-66-N=IM (blue) and **D-UiO-66-N=IM** (green) measured at 77 K.

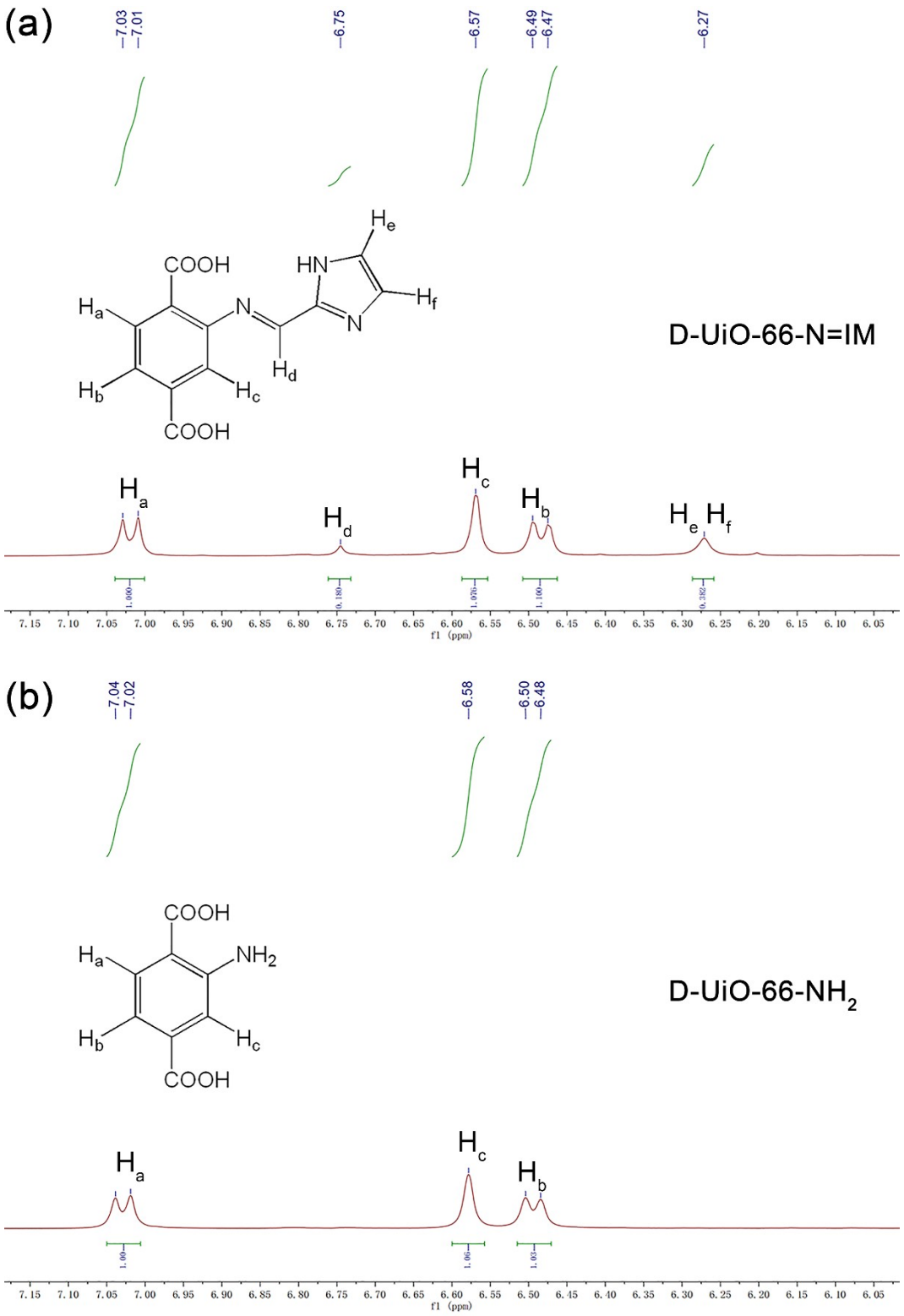

Fig. S2. Dissolution/^{1}H NMR spectra of **D-UiO-66-N=IM** (a) and D-UiO-66-NH_2 (b) with NaOD as digestion solvent and 400 MHz as spectrometer frequency.

According to the signal peaks and corresponding integrations in D-UiO-66-NH_2, H_a:H_b:H_c = 1:1:1. The number of missing linkers in D-UiO-66-NH_2 is 0.74. The total

numbers of (H_a + H_b +H_c) in each MOF unit ($Zr_6O_4(OH)_4(BDC\text{-}NH_2)_6$) in D-UiO-66-$NH_2$ is 15.78. In D-UiO-66-N=IM, H_a:H_b:H_c:H_d = 1:1:1:0.2. Therefore, the number of introduced imidazole units in each MOF unit is 1.05.

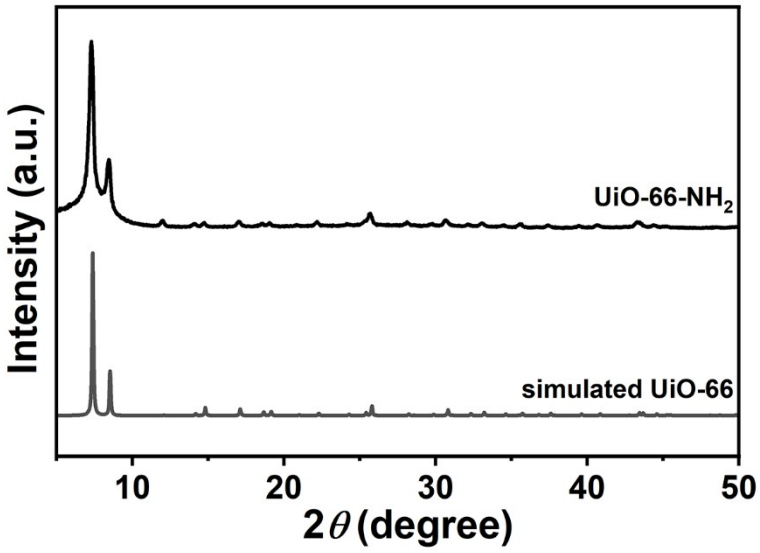

Fig. S3. PXRD patterns of simulated UiO-66 (gray) and as-synthesized UiO-66-NH_2 (black).

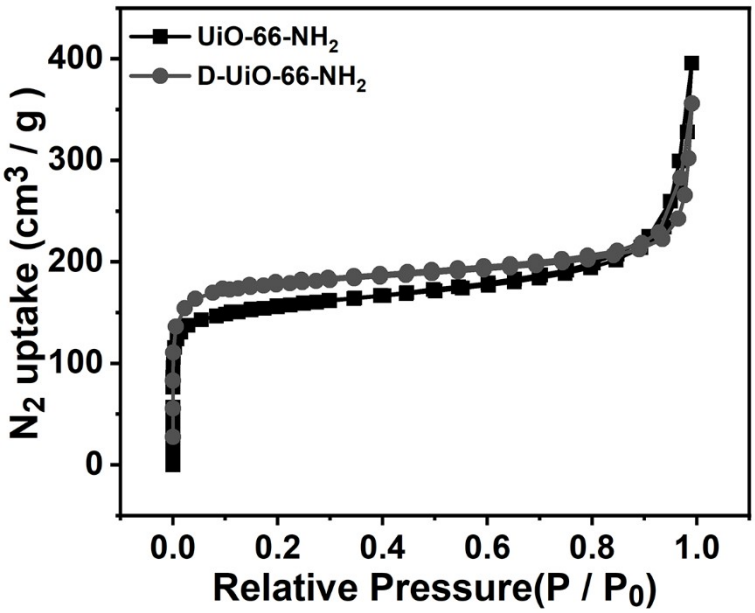

Fig. S4. N_2 adsorption-desorption isotherms of UiO-66-NH_2 (black) and D-UiO-66-NH_2 (gray) measured at 77 K.

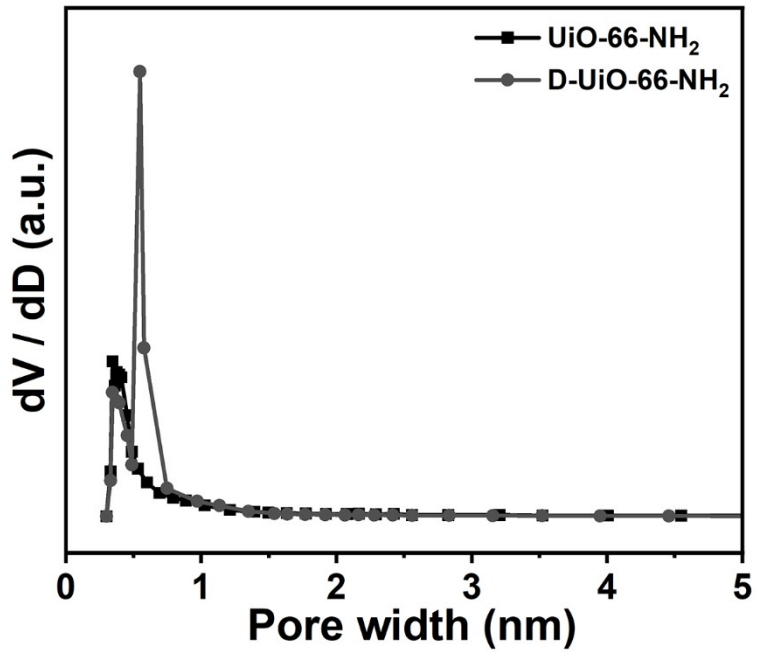

Fig. S5. The pore size distribution curves of UiO-66-NH_2 (black) and D-UiO-66-NH_2 (gray).

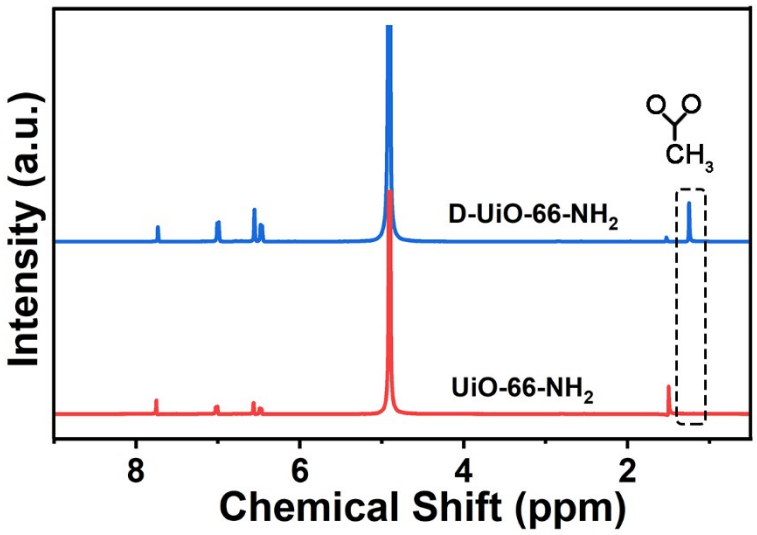

Fig. S6. Dissolution/^{1}H NMR spectra of UiO-66-NH_2 (red) and D-UiO-66-NH_2 (blue) with NaOD as digestion solvent and 400 MHz as spectrometer frequency.

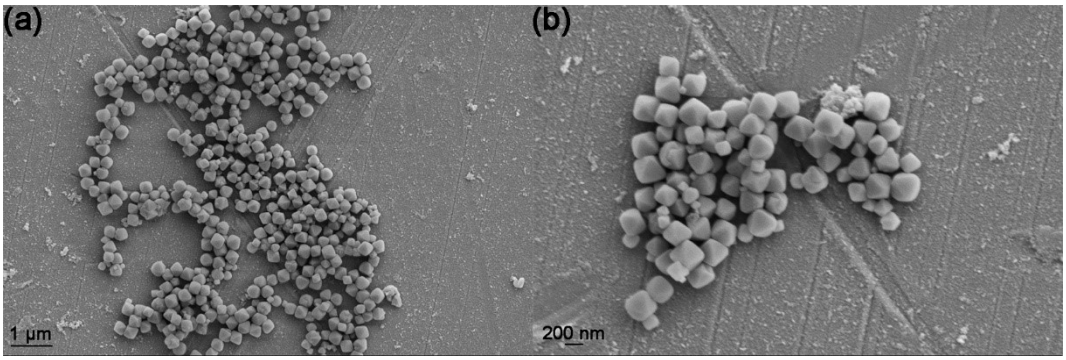

Fig. S7. The typical SEM images of D-UiO-66-NH_2.

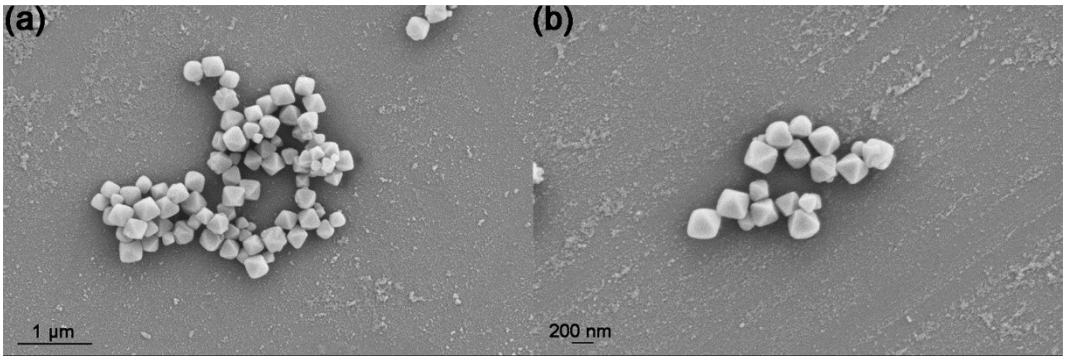

Fig. S8. The typical SEM images of UiO-66-N=IM.

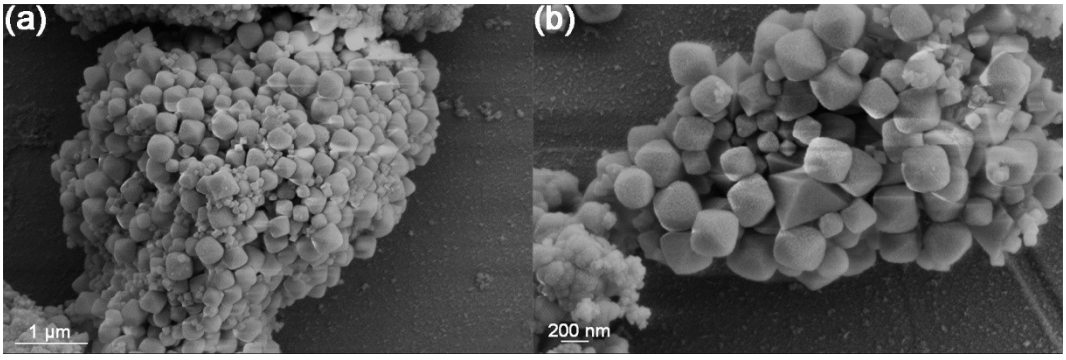

Fig. S9. The typical SEM images of **D-UiO-66-N=IM**.

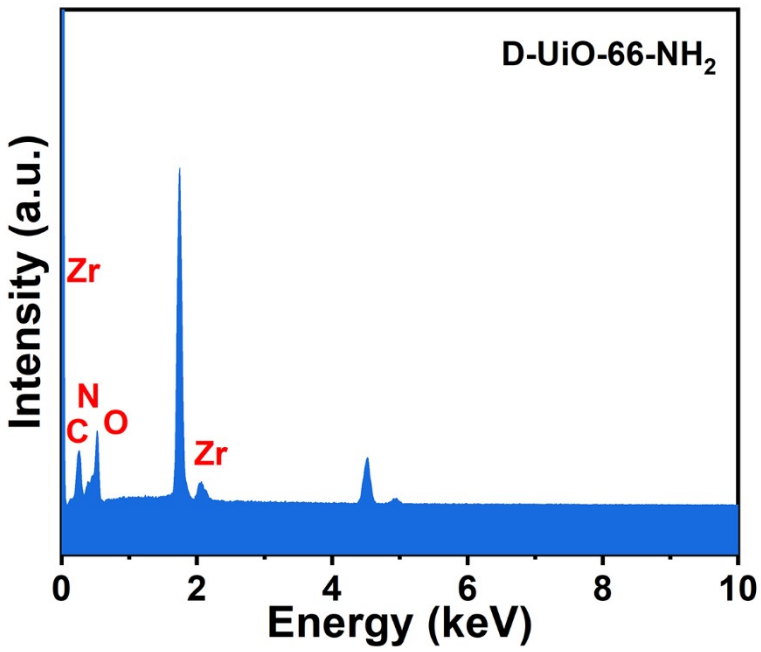

Fig. S10. Energy-dispersive X-ray (EDX) spectrum of D-UiO-66-NH_2.

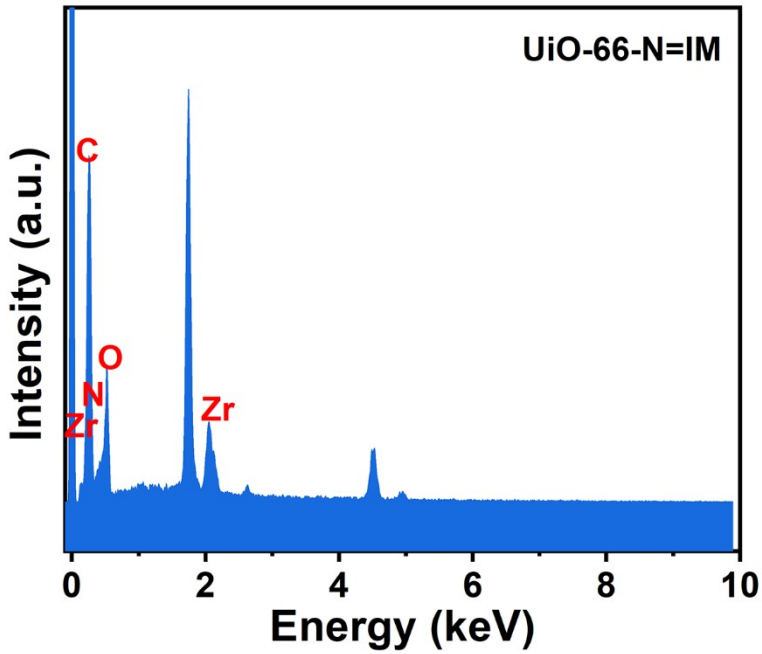

Fig. S11. Energy-dispersive X-ray (EDX) spectrum of UiO-66-N=IM.

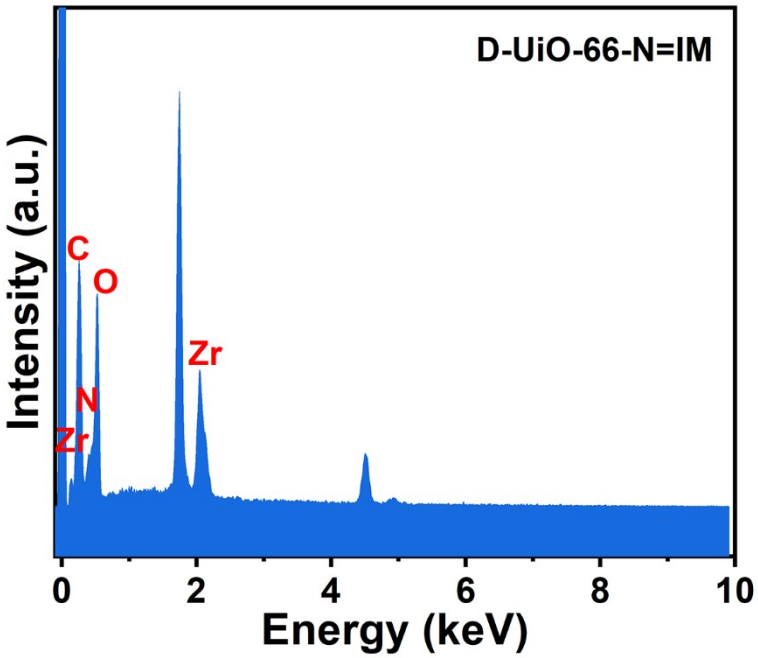

Fig. S12. Energy-dispersive X-ray (EDX) spectrum of **D-UiO-66-N=IM**.

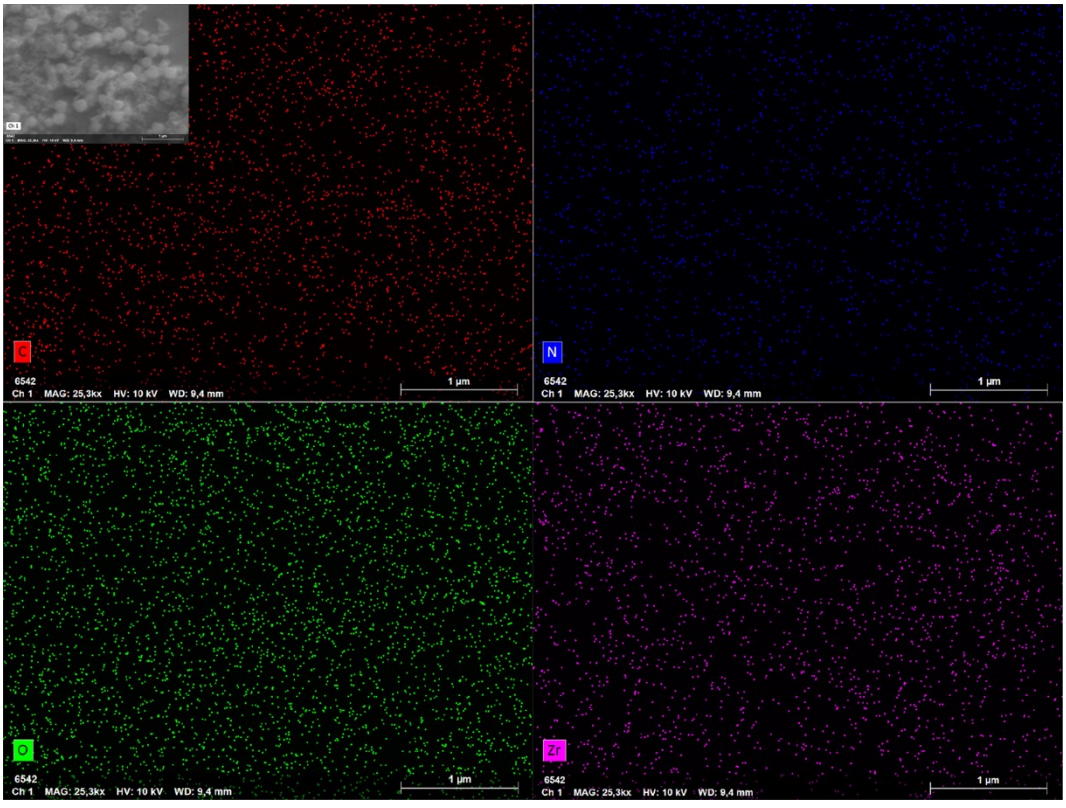

Fig. S13. EDX maps of D-UiO-66-NH_2.

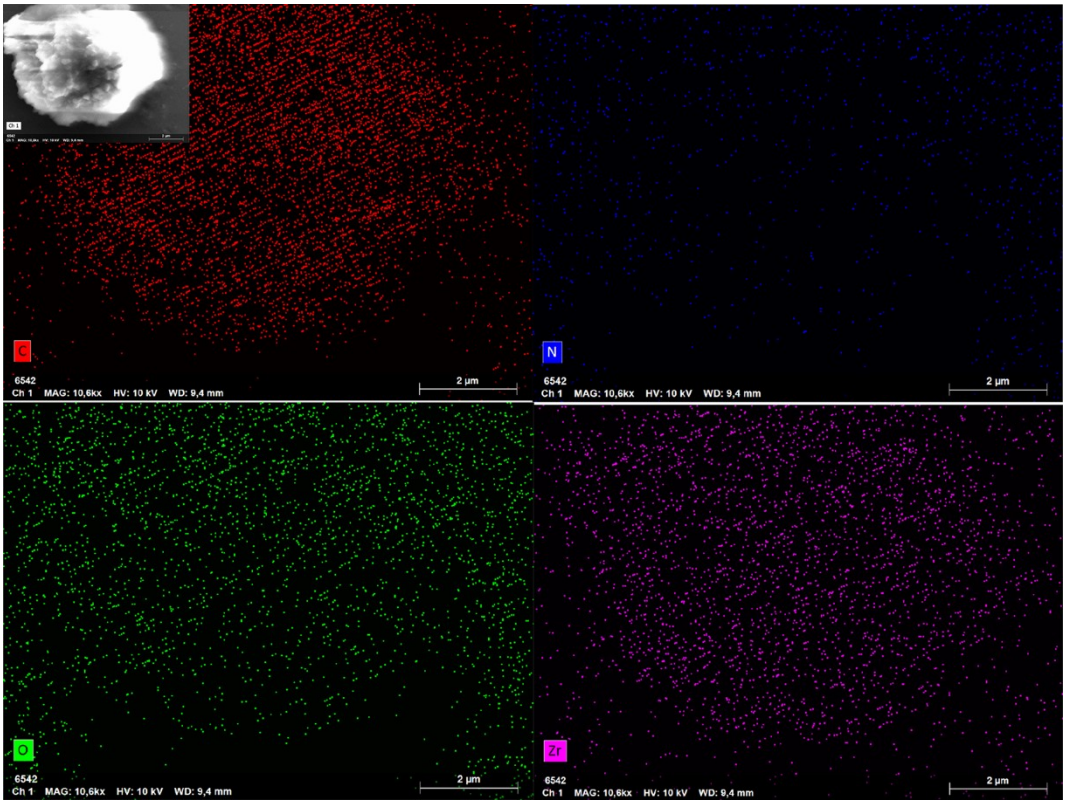

Fig. S14. EDX maps of UiO-66-N=IM.

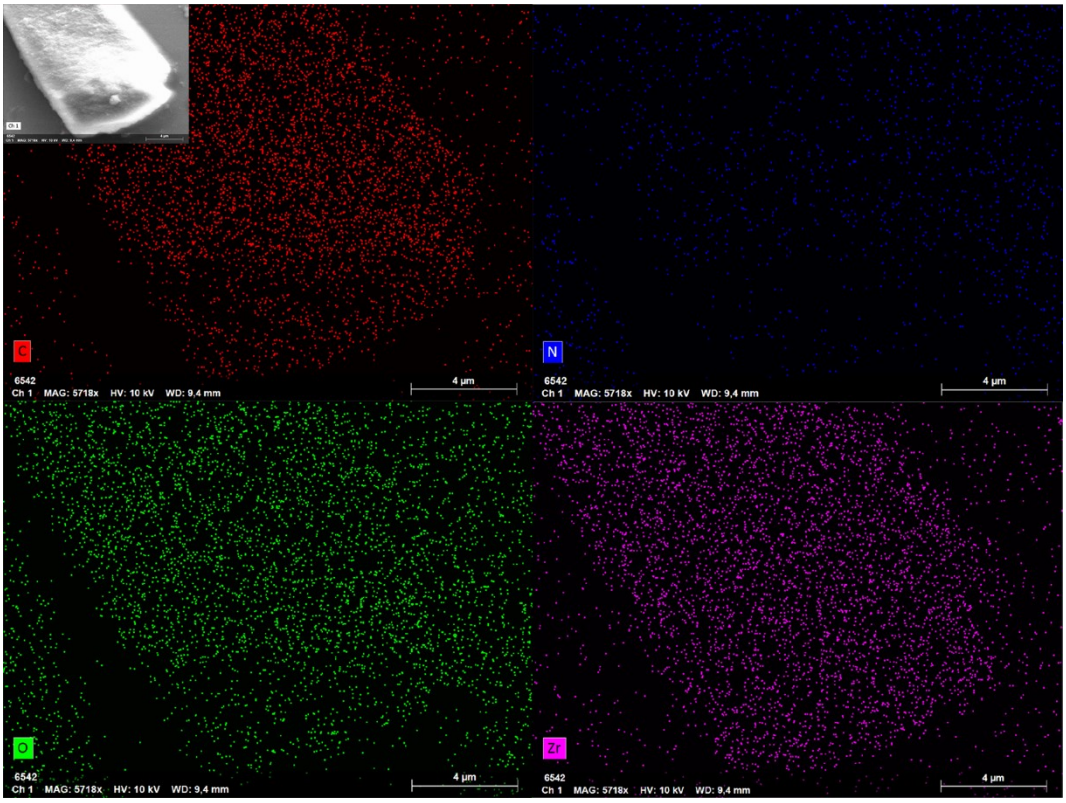

Fig. S15. EDX maps of **D-UiO-66-N=IM**.

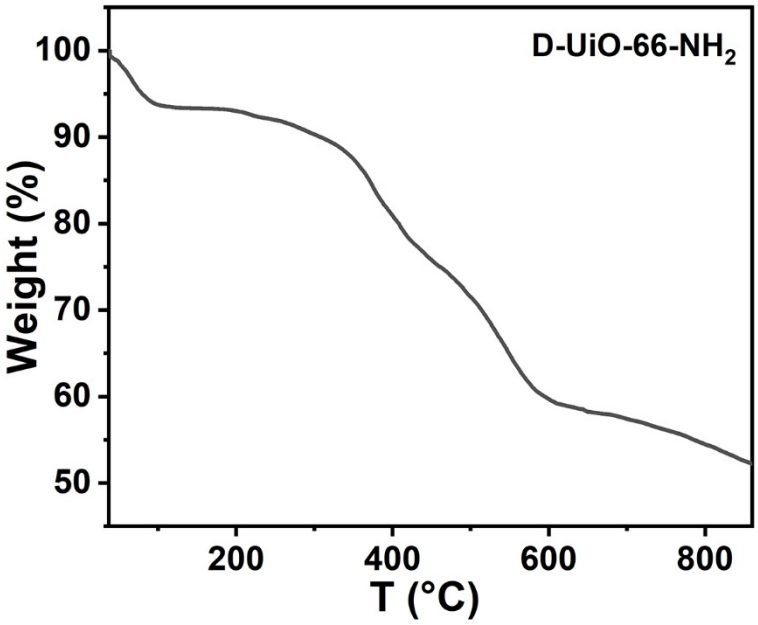

Fig. S16. TGA curve of D-UiO-66-NH_2.

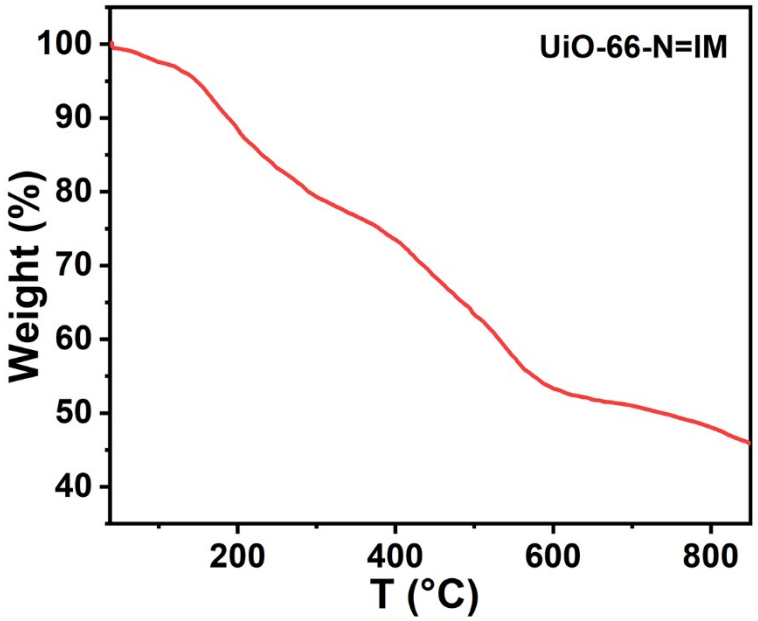

Fig. S17. TGA curve of UiO-66-N=IM.

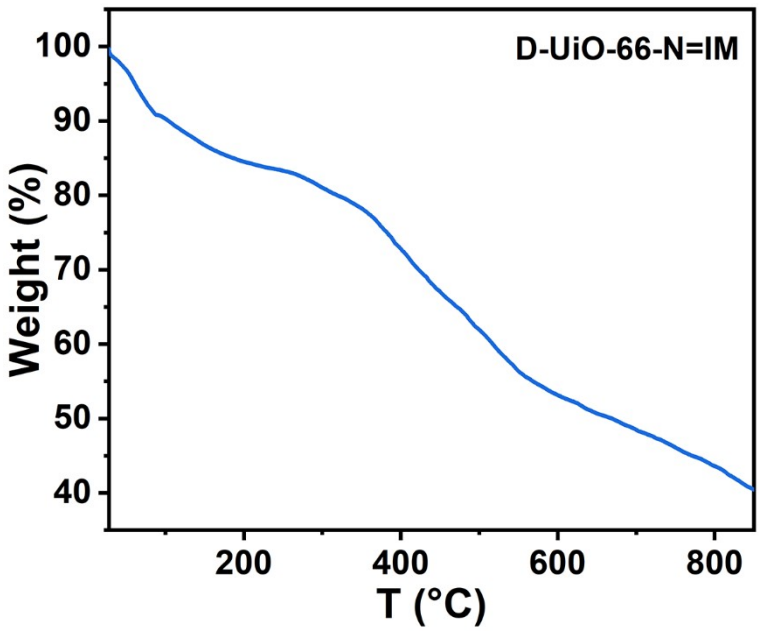

Fig. S18. TGA curve of **D-UiO-66-N=IM**.

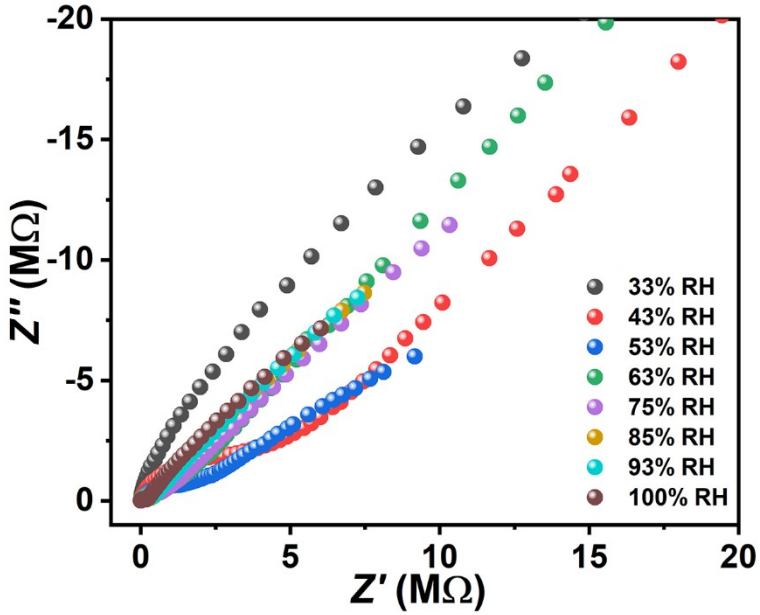

Fig. S19. Nyquist plots of D-UiO-66-NH_2 at room temperature and different humidities variation from 33% to 100% RH.

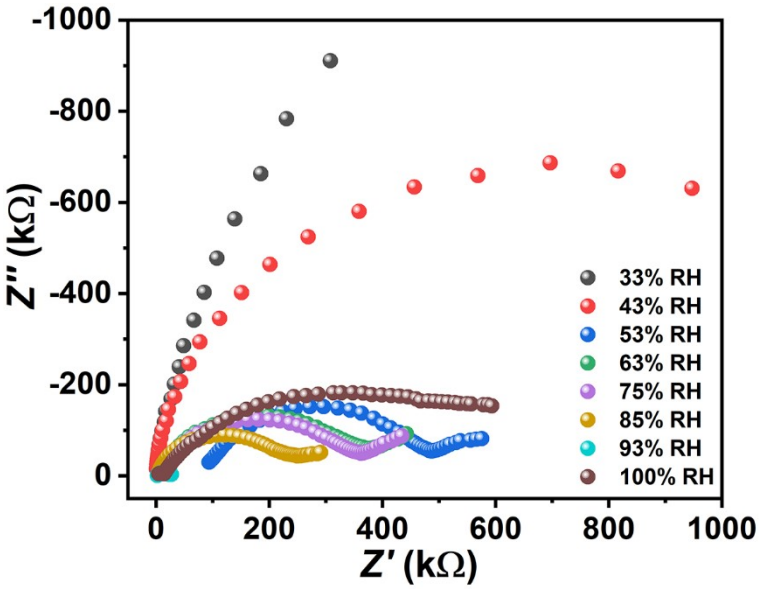

Fig. S20. Nyquist plots of UiO-66-N=IM at room temperature and different humidities variation from 33% to 100% RH.

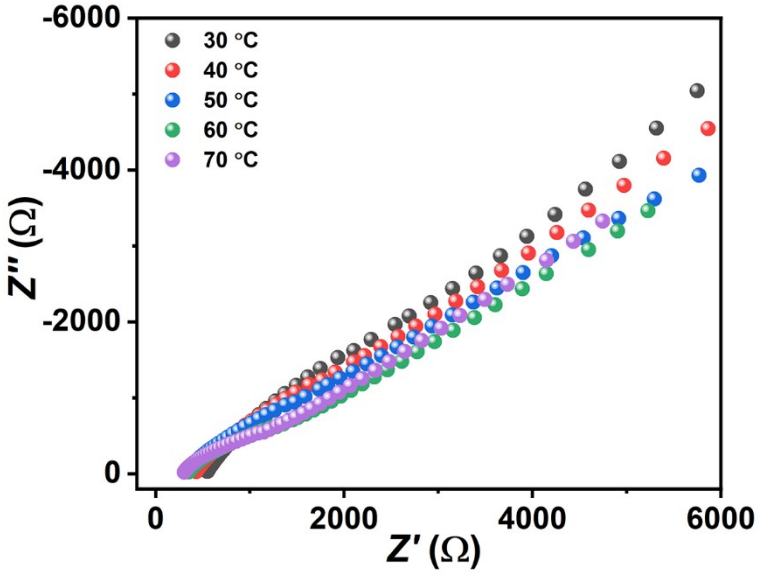

Fig. S21. Nyquist plots of D-UiO-66-NH_2 at 100% RH and different temperatures variation from 30 to 70 ℃.

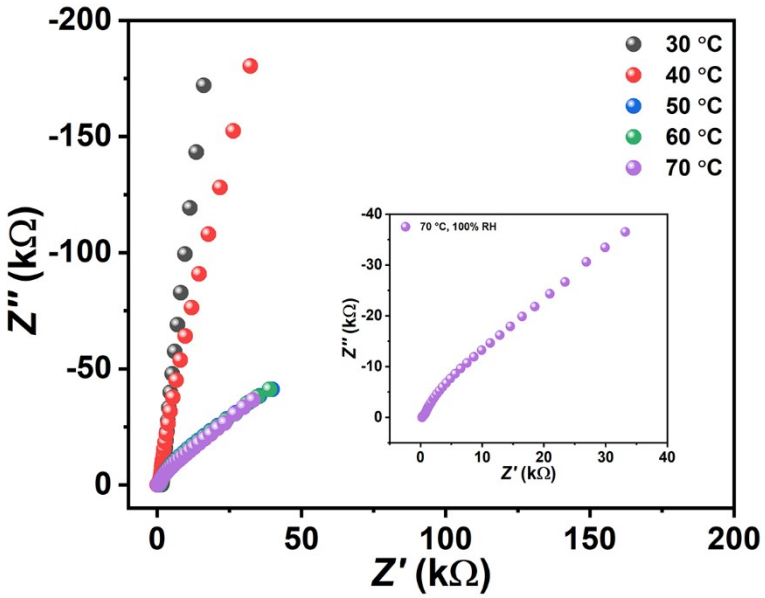

Fig. S22. Nyquist plots of UiO-66-N=IM at 100% RH and different temperatures variation from 30 to 70 ℃.

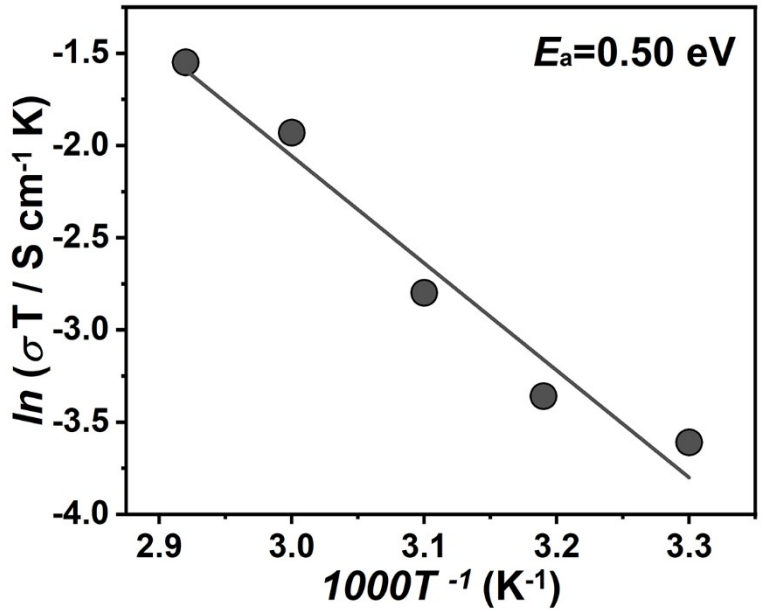

Fig. S23. Arrhenius plot of D-UiO-66-NH_2 under 100% RH and in the temperature range of 30-70 ℃.

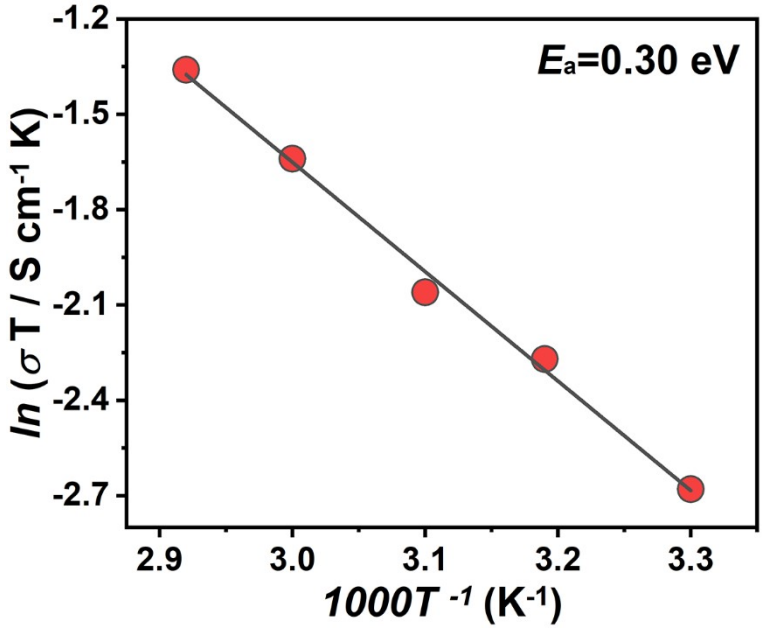

Fig. S24. Arrhenius plot of UiO-66-N=IM under 100% RH and in the temperature range of 30-70 ℃.

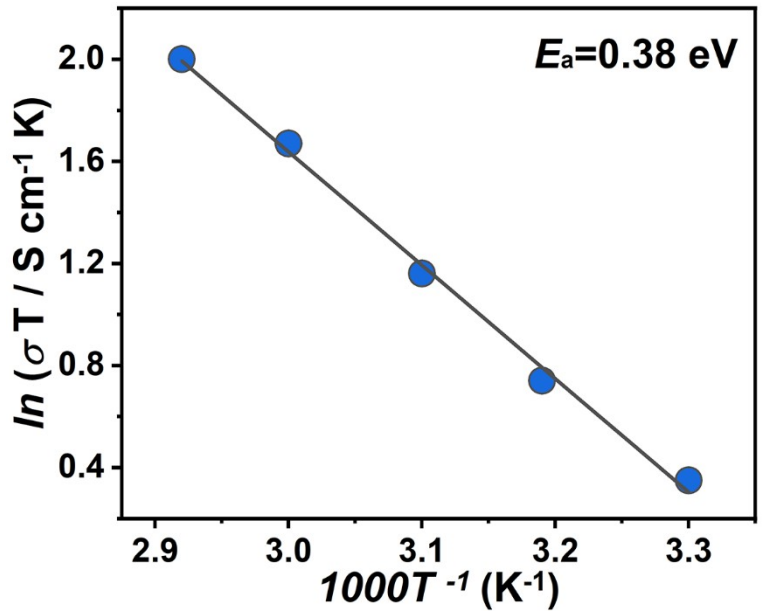

Fig. S25. Arrhenius plot of **D-UiO-66-N=IM** under 100% RH and in the temperature range of 30-70 ℃.

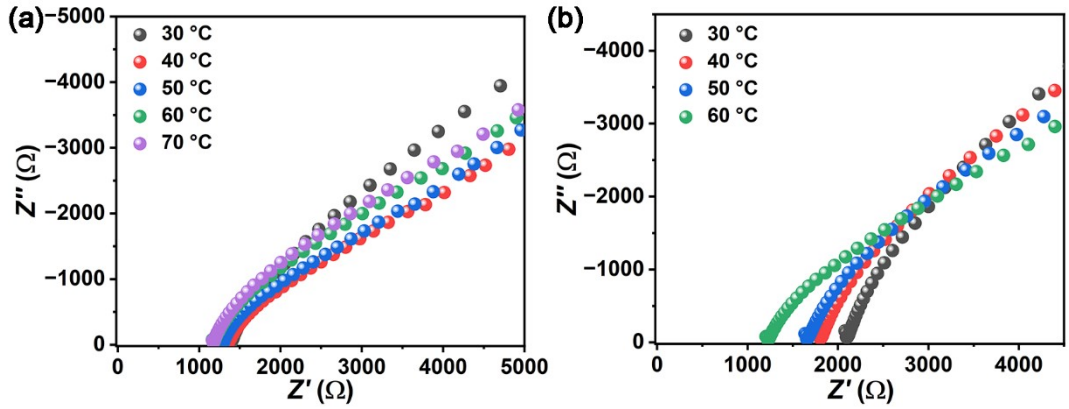

Fig. S26. Nyquist plots of **D-UiO-66-N=IM** for the heating-cooling cycle under 100% RH: (a) the heating cycle (30-70 ℃); (b) the cooling cycle (60-30 ℃).

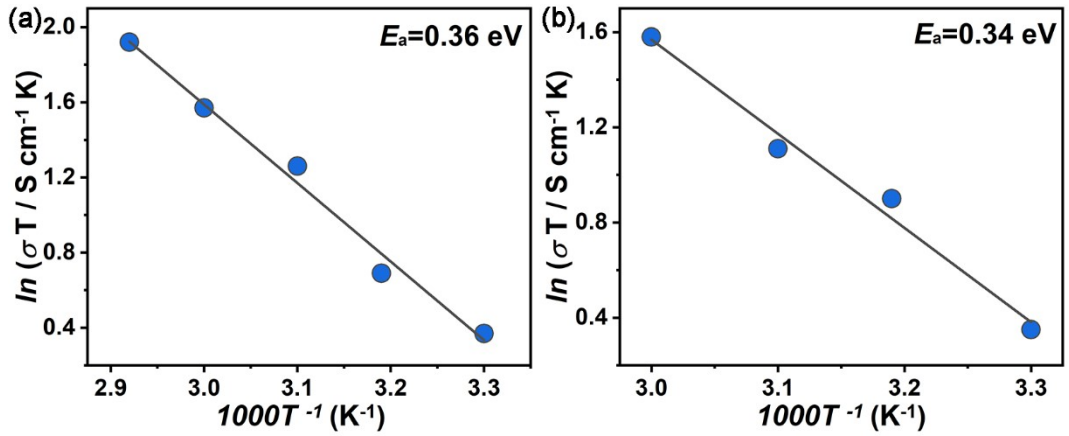

Fig. S27. Arrhenius plots of **D-UiO-66-N=IM** for heating-cooling cycle at the temperature range of 30-70 ℃ and 100% RH: (a) the heating cycle (30-70 ℃); (b) the cooling cycle (60-30 ℃).

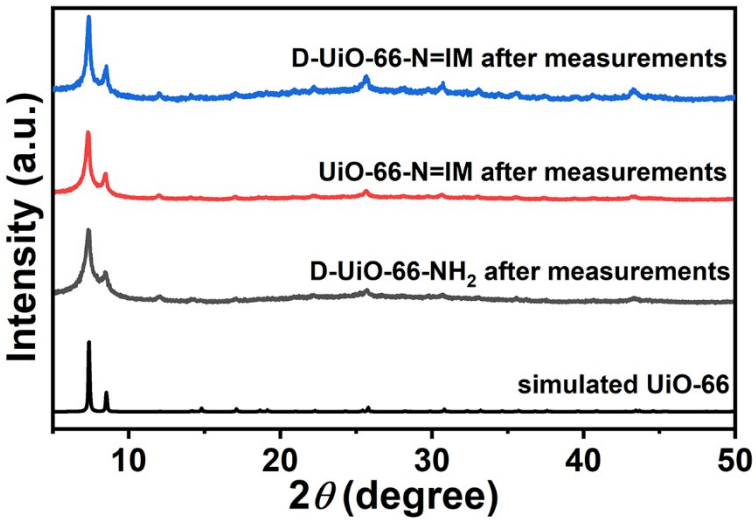

Fig. S28. PXRD patterns of simulated UiO-66 (black), D-UiO-66-NH_2 after proton conduction measurements (gray), UiO-66-N=IM after proton conduction measurements (red) and **D-UiO-66-N=IM** after proton conduction measurements (blue).

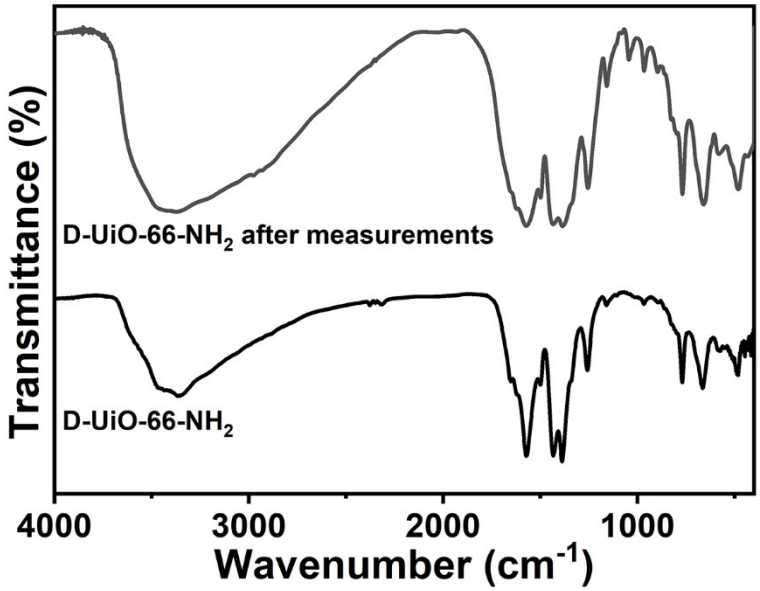

Fig. S29. FTIR spectra of as-synthesized D-UiO-66-NH_2 (black) and D-UiO-66-NH_2 after proton conduction measurements (gray).

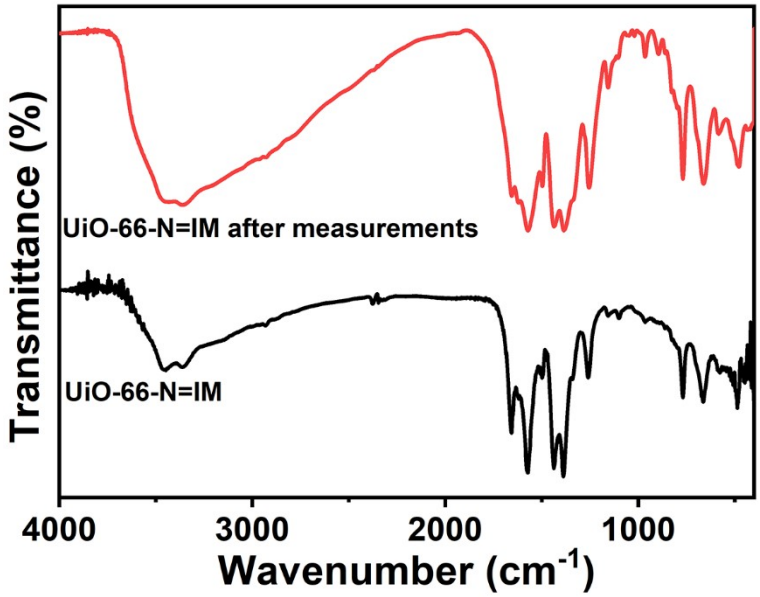

Fig. S30. FTIR spectra of as-synthesized UiO-66-N=IM (black) and UiO-66-N=IM after proton conduction measurements (red).

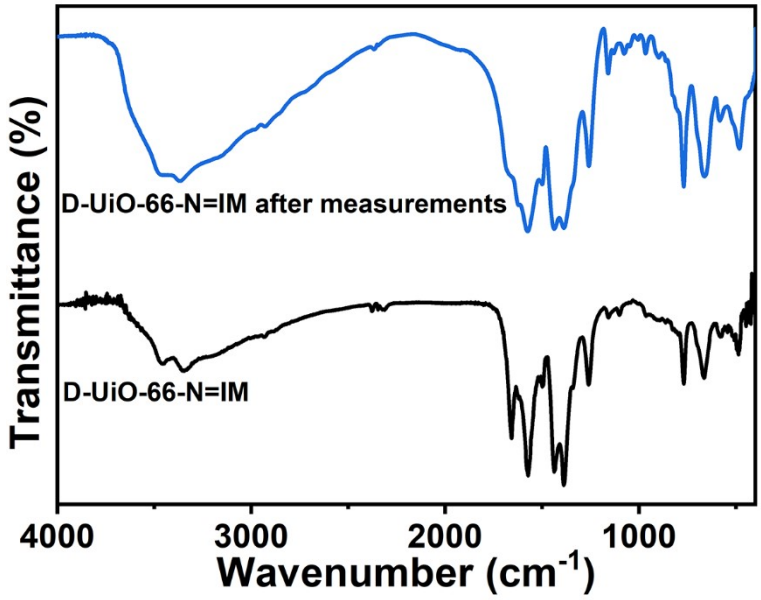

Fig. S31. FTIR spectra of as-synthesized D-UiO-66-N=IM (black) and D-UiO-66-N=IM after proton conduction measurements (blue).

Table S1. Comparison of proton conductivities and preparation strategies of **D-UiO-66-N=IM** and some other representative MOFs-based proton conductors measured under hydrous condition (Ligand Modification = 1, Defect Engineering = 2).

Compound	Condition		σ (S cm^{-1})	Preparation Strategy	Reference
	T (℃)	RH			
Im-Fe-MOF	60	98%	1.21×10^{-2}	1	4
MOF-808-IMDC	80	98%	1.11×10^{-2}	1	5
UiO-66-COOH-Asp	70	98%	1.19×10^{-2}	1	6
Cd-5TIA	28	98%	3.61×10^{-3}	1	7
MIL-53(Fe)-$(COOH)_2$	80	95%	7×10^{-4}	1	8

Im-Cu@NENU-3a	70	90%	3.16×10^{-4}	1	9
MOF-808D	80	98%	1.12×10^{-2}	2	10
MOF-808C	80	98%	2.6×10^{-1}	2	10
TMOF-2	90	98%	1.23×10^{-4}	2	11
$Zr_6O_4(OH)_6(O_2C\text{-}C_6H_4\text{-}CO_2)_5$	65	95%	6.93×10^{-3}	2	12
Sulfonated zirconium terephthalate	65	95%	1.92×10^{-3}	2	13
D-UiO-66-N=IM	70	100%	2.15×10^{-2}	1 and 2	This work

Reference

1. C. Gomes Silva, I. Luz, F. X. Llabrés i Xamena, A. Corma and H. García, *Chem. Eur. J.*, 2010, **16**, 11133-11138.

2. X. Ma, L. Wang, Q. Zhang and H.-L. Jiang, *Angew. Chem., Int. Ed.*, 2019, **58**, 12175-12179.

3. S.-Y. Zhu and B. Yan, *Dalton Trans.*, 2018, **47**, 11586-11592.

4. F.-M. Zhang, L.-Z. Dong, J.-S. Qin, W. Guan, J. Liu, S.-L. Li, M. Lu, Y.-Q. Lan, Z.-M. Su and H.-C. Zhou, *J. Am. Chem. Soc.*, 2017, **139**, 6183-6189.

5. X.-M. Li, Y. Wang, Y. Mu, J. Gao and L. Zeng, *J. Mater. Chem. A*, 2022, **10**, 18592-18597.

6. X.-M. Li, J. Jia, D. Yang, J. Jin and J. Gao, *Chinese Chem. Lett.*, 2024, **35**, 108474.

7. T. Panda, T. Kundu and R. Banerjee, *Chem. Commun.*, 2012, **48**, 5464-5466.

8. A. Shigematsu, T. Yamada and H. Kitagawa, *J. Am. Chem. Soc.*, 2011, **133**, 2034-2036.

9. Y. Ye, W. Guo, L. Wang, Z. Li, Z. Song, J. Chen, Z. Zhang, S. Xiang and B. Chen, *J. Am. Chem. Soc.*, 2017, **139**, 15604-15607.

10. O. Basu, S. Mukhopadhyay, S. Laha and S. K. Das, *Chem. Mater.*, 2022, **34**, 6734-6743.

11. G. Zhang and H. Fei, *Chem. Commun.*, 2017, **53**, 4156-4159.

12. J. M. Taylor, S. Dekura, R. Ikeda and H. Kitagawa, *Chem. Mater.*, 2015, **27**, 2286-2289.

13. J. M. Taylor, T. Komatsu, S. Dekura, K. Otsubo, M. Takata and H. Kitagawa, *J. Am. Chem. Soc.*, 2015, **137**, 11498-11506.